Journal of Alloys and Compounds 834 (2020) 155173

Contents lists available at ScienceDirect

Journal of Alloys and Compounds

journal homepage: http://www.elsevier.com/locate/jalcom

Effect of oxygen on microstructural coarsening behaviors and mechanical properties of Ag sinter paste during high-temperature storage from macro to micro

Chuantong Chen [a, *], Chanyang Choe [a, b], Dongjin Kim [a, b], Zheng Zhang [a, b], Xu Long [c], Zheng Zhou [d], Fengshun Wu [d], Katsuaki Suganuma [a]

[a] The Institute of Scientific and Industrial Research, Osaka University, Ibaraki-shi, Osaka, 567-0047, Japan
[b] Department of Adaptive Machine Systems, Osaka University, Osaka, 567-0571, Japan
[c] School of Mechanics, Civil Engineering and Architecture, Northwestern Polytechnical University, Xi'an, 710072, China
[d] School of Materials Science and Engineering, Huazhong University of Science and Technology, Wuhan, 430074, China

ARTICLE INFO

Article history:
Received 18 February 2020
Received in revised form
10 April 2020
Accepted 11 April 2020
Available online 18 April 2020

Keywords:
Ag sinter paste
Coarsening behavior
Fracture behaviors
Ag-O reaction
Micromechanical properties
High-temperature aging

ABSTRACT

This study systematically investigates the effect of oxygen on the microstructural evolution as well as the macro/micromechanical characterization of Ag sinter paste during the aging process at 250 °C for 1000 h. The sintered Ag joint is separated into two groups and, respectively, kept in air and vacuum (10^{-4} Pa) atmospheres. The microstructure of sintered Ag paste become clearly coarsened after aging at 250 °C in air for 100 h, while it remains almost the same as in the initial state in vacuum, even after aging for 1000 h. The different microstructural evolutions are investigated in detail by transmission electron microscopy, which reveals that coarsening are involved in the Ag-O reaction and form a large number of Ag nanoparticles around sintered Ag particles, as well as enhance coalescence. Furthermore, the macro/micromechanical properties of sintered Ag paste, after aging in air and vacuum atmospheres, are evaluated by a die shear test and a nano-indenter system with a spherical diamond tip. Shear strength and fracture mode were systematically analyzed. The micromechanical properties of sintered Ag paste, including Young's modulus and hardness, depend on its microstructure and are largely influenced by its porosity, which decreases from initiation to 250 h and recovers after aging for 500 h in air. However, there is almost no change during the aging process in the vacuum atmosphere. The results of this study contribute to a better understanding of the microstructural evolution and the mechanical properties of sintered Ag joints, including the change in bonding quality and Young's modulus during aging for actual power modules, which are packaged by a resin.

1. Introduction

SiC power devices are shown to have excellent properties for required high power density devices in the automobile industry through electric vehicles and hybrid electric vehicles. It can work well at high temperature above 250 °C, which is extremely attractive for power applications [1–3]. In the SiC power modules, Ag sinter paste joining technology has become a potential candidate to replace solder technology due to its high melting point (961 °C), excellent electrical and thermal conductivity [4–9] as well as a crack self-healing functions in high-temperature storing [10]. In addition, thermomechanical reliability of sinter Ag joint has been improved recently during a harsh thermal shock environment from −50 °C to 250 °C [11,12].

Unlike in the traditional soldering process, Ag sinter paste are formed through solvent wetting, evaporation, and a process of solid diffusion of Ag atoms, wherein they usually exhibit a nano- or micro-porous structure [13,14]. Such microstructures are typically thermodynamically unstable at high-temperature services, such as high-temperature aging. Sintered Ag paste tend to coarsen rapidly during aging at high temperatures, while the pore size and numbers decrease simultaneously with shape change at high temperatures due to Oswald ripening [15–19]. The microstructural evolution is called "coarsening behaviors" of the sintered Ag porous

* Corresponding author.
E-mail address: chenchuantong@sanken.osaka-u.ac.jp (C. Chen).

https://doi.org/10.1016/j.jallcom.2020.155173
0925-8388/

structure. Indeed, coarsening behaviors are particularly important for the mechanical, electrical, and thermal properties of sintered Ag joint [20–22]. For example, the decreasing porosity and Ag particle sizes of the sintered joint always leads to an increase of the elastic modules, yield stress, and shear strength. The changes in pore sizes and their distribution also influence the formation and growth rate of cracks due to the change in the distribution of thermal stress in the sintered Ag joint. Thus, a better understanding of coarsening behaviors of sintered porous Ag structure is very essential for its reliable application and life time evaluation in electric devices.

Normally, the Ag particle and pore coarsening of sintered Ag paste are dependent on the aging temperature. Although, the particle sizes and pore sizes do not significantly change under aging at lower temperatures, such as 125–150 °C, they become coarsened at temperatures above 250 °C. Thus, most studies concluded that the thermal self-diffusion of Ag was attributed to the coarsening behaviors of sintered Ag paste during high-temperature aging [15,17,23]. However, recent studies have revealed that Ag atoms have a special reaction with oxygen due to the thermal instability of Ag_2O [24–26], and this reaction has a close relationship with physical phenomena such as the self-generation of Ag nanoparticles [27–29], self-healing process [10], and formation of Ag hillocks during the heating process [30,31]. Therefore, the coarsening behaviors may be more complex than just the self-diffusion of Ag atoms and may be largely influenced by the reaction between the oxygen atmosphere and Ag during high temperatures. However, in the actual power modules, which are packaged by resins after die attach bonding, the microstructural evolution, including coarsening behaviors, is not influenced by oxygen. The study of power modules under vacuum atmospheres during high-temperature aging is beneficial to understand the microstructural evolution and bonding quality change for the actual power modules, as well as the oxygen effect on both phenomena.

Additionally, recent studies show that the micromechanical properties and fracture behaviors of sintered porous Ag largely depend on its microstructure [32,33], which relates not only on its porosity but also upon the degree of necking growth among the Ag particles [34]. Due to the micromechanical properties of the sintered Ag paste during high-temperature aging should largely influenced by its microstructure evolution, micromechanical properties evaluation with aging time changed to an imminent issue for the accurate left-time prediction of electrical devices. For the sintered Ag paste with the nano- or micro-porous structure, few studies focus on the properties of the microscale materials due to the complex fracture behaviors, which were different with the dense metallic structure, wherein dislocation or slipping behaviors were less evident during a micro-scaled compression test [34]. Additionally, the traditional nano-indentation tests by a diamond tip with a known geometry (conical, spherical, or pyramidal indenter) for the microscale dense metallic structure have already been studied for many years [35–38]. Recently, the nano-indentation test was also used on sintered Ag porous structures to obtain their micromechanical properties [39,40]. However, information on the micromechanical properties of sintered porous Ag during high-temperature aging are unavailable, especially the evaluation of the effect of oxygen on the micromechanical properties.

Herein, we investigate the effect of oxygen on both the microstructural evolution and mechanical properties of sintered Ag joints, which remain during high-temperature aging in air and in vacuum atmospheres. The aging temperature is selected as 250 °C, which is similar to the junction temperature of real WBG power devices. This study also focuses on the mechanism of the oxygen involvement in coarsening behaviors during high-temperature aging in the die-attached module structure, which are systemically discussed by scanning electron microscopy (SEM), energy dispersive x-ray spectroscopy (EDS), and transmission electron microscopy (TEM) analyses. Furthermore, the micromechanical properties of sintered Ag paste after aging in air and in vacuum atmospheres are evaluated by a nano-indenter system with a spherical diamond tip. The relationship between the microstructural and micromechanical properties of sintered Ag paste is also systematically analyzed in detail.

2. Experimental process

2.1. Ag paste and sinter Ag joining

In the experiment, Ag fillers were composited by submicron-sized Ag particles as shown in Fig. 1(a). Fig. 1(b) shows the relationship between the volume of the relative particles and Ag particles size. The fillers were then mixed with an ether-type solvent ($C_xH_yO_z$, $x > 10$, with a boiling point of approximately 200 °C, Daicel Corporation) with a weight percentage of 10% by a hybrid mixer (HM-500, Keyence Corporation, Japan) to fabricate an Ag paste. Termogravimetry (TG) and differential thermal analysis (DTA, 2000SE Netzsch, Selb, Germany) curves of the Ag paste in the static air atmosphere were measured, where the weight loss is mainly detected from 50 °C to 130 °C, and slightly decreased from 130 °C to 260 °C. The DTA curve presents a tiny exothermic peak at approximately 130 °C and a huge exothermic peak around 260 °C (see supporting information F. S1). For the tiny exothermic peak, it may be attributed to the combustion of organic compounds to cause a small weight loss. For the huge exothermic peak, a possible explanation is that the solvents reacted with the dispersant on the surface of Ag particles under heating, or with silver catalyst to produce high-molecular-weight compounds to be decomposed/burned at high temperature, leading to weight loss and an exothermic phenomenon [41–43]. The prepared Ag paste, with the dimensions of 3 mm × 3 mm × 0.1 mm was screen-printed onto Direct bonded copper (DBC, $Cu/Si_3N_4/Cu$) substrates in the dimensions of 10 mm × 10 mm × 1.23 mm, and then SiC dies in the dimensions of 3 mm × 3 mm × 0.35 mm were placed on the paste. Both the back side of SiC chips and the top side of DBC substrates were plated in order with a 200 nm Ti layer and 1 μm Ag layer via a sputtering process. The schematic representation of the experimental processes was shown in Fig. 1(c–f). Finally, these samples were heated on a hotplate under 250 °C for 30 min without any extra pressure in air as seen in Fig. 1(g). Subsequently, the sintered Ag joints were aged at 250 °C for 1000 h in air and vacuum atmospheres with a vacuum degree of 10^{-4} Pa.

2.2. Mechanical evaluation

After the aging test in air and vacuum atmospheres, the die shear strength of the sintered Ag joint structure was evaluated by a shear tester (Dage 4000, Japan) with the shear speed at 50 μm/s. Seven SiC joint structures were evaluated to get the average shear strength on each condition. Additionally, to evaluate the micromechanical properties of sintered Ag paste after aging in the air and vacuum atmospheres, the Ag paste was printed on glass substrates with the same sintering procedure as introduced in Section 2.1. The Ag paste had the same dimensions (3 mm × 3 mm × 0.1 mm) as the sinter Ag joint. Afterward, the sintered Ag paste was aged at 250 °C in air and vacuum atmospheres for 1000 h. Next, the sintered Ag paste were slightly mechanically ground and polished with a 4000 grit SiC paper. The micromechanical properties of the sintered Ag paste, before and after aging in air and vacuum atmospheres for 200 h, 500 h, and 1000 h were evaluated by a nano-indenter system (Ti950, Hysitron) with a spherical diamond tip, which has a diameter of 2 μm. Compared to sharp indenters, including

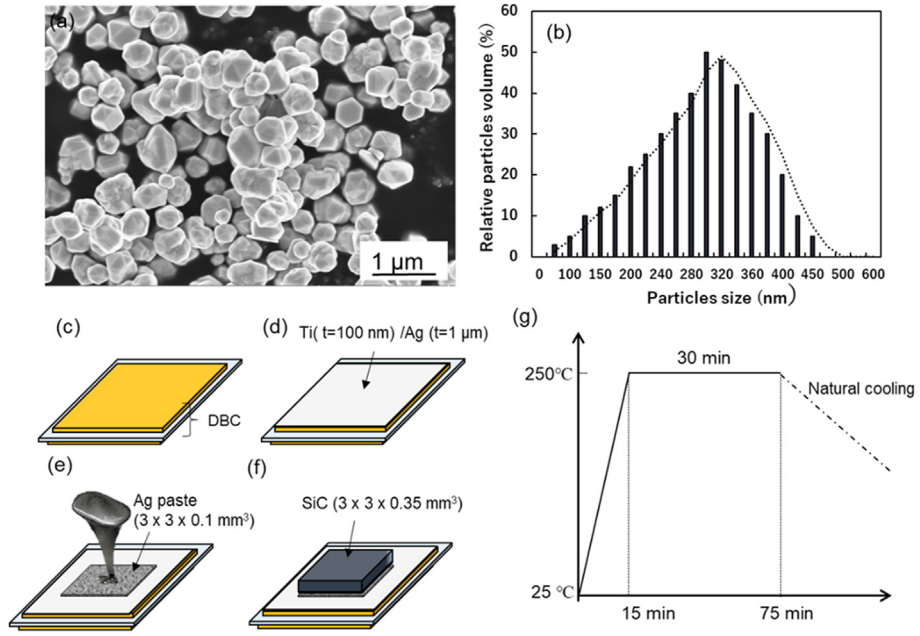

Fig. 1. (a) SEM image of submicron-scale Ag particles, (b) the particles size distribution, (c) preparation of DBC substrate, (d) sputtering Ti/Ag layer on the DBC substrate, (e) printing Ag paste after sputtering, (f) mounting the SiC chip on the paste and (g) the sintering process in air without assistant pressure.

berkovich tips, spherical tips facilitate the distinction between elastic and plastic deformation of materials during indentation due to their less drastic variation of stress under loading [44,45]. During the test, the nano-indentation was load-controlled for each specimen. The time to maximally load was set as 10 s, while load removal time was also 10 s. The maximum load was set as 8000 μN for all the samples, and five places were implemented on each sample. The Young's modulus of the diamond tip is 1140 GPa, and the Poisson's ratio is 0.07. The load and displacement curve can be recorded during the test.

2.3. Characterization analysis

To investigate the evolution of microstructure of sintered Ag joint during high temperature in air and vacuum, cross-section of the sintered Ag joint was prepared by an ion milling polishing machine (IM 4000; Hitachi, Japan). The evolution of microstructure of sintered Ag joint was observed using scanning electron microscopy (SEM, SU-8020; Hitachi, Japan). The particle coarsening mechanism in air and vacuum was analyzed by transmission electron microscopy (TEM, JEM-ARM200F, JOEL, Japan) at 200 KV. To better understanding the fracture behavior and response during nano-indentation test for the sintered Ag paste aged in air and in vacuum, the locations of nano-indentation test were cut by a Focused ion beam (FIB, FIB-2100, HITACHI) by a finer milling current (40 keV, 0.36 nA).

3. Results and discussions

3.1. Microstructural characterization

3.1.1. Particle coarsening behaviors

Fig. 2(a) shows the SEM images of the initial microstructure of the sintered Ag joint, and Fig. 2(b), (c), and (d) show the magnified views at the interface of the SiC and sintered porous Ag, the sintered porous Ag layer, and the interface of the sintered porous Ag and Cu substrate, respectively. Fig. 2(e) and (i) show the microstructural evolution of the sintered Ag joint after aging at 250 °C for 500 h in air and in vacuum, respectively. At the initial state, the sintered Ag paste appeared as a porous network. After aging for 500 h in air, the sintered Ag paste appeared as a coarsening phenomenon, where the both particles and pores were enlarged, as reported in our previous studies [46,47].

Fig. 2(f), (g), and (h) show the magnified views at the interface of SiC and sintered Ag paste, sintered Ag paste, and the interface between the sintered Ag paste and DBC substrate in air atmosphere, respectively. As clearly shown in Fig. 2(f) and (h), the Ag metallization layers on both the SiC chip and DBC substrate were diffused into the sintered Ag paste, leading to the latter directly contacting with the Ti layer, which was a dewetting phenomenon from Ti layer [46,47]. The diffusion of the Ag metallization layer may also improve the coarsening behavior of sintered Ag paste. The reason may be explained by when coarsening was continuously triggered at 250 °C, Ag atoms in the Ag metallization layer were passively absorbed into the porous Ag to support the coarsening process due to stress migration [48]. Furthermore, when polycrystalline materials are exposed to high temperatures, the grain growth to reduce the interfacial energy of numerous grain boundaries through their migration [49].

On the other hand, during this coarsening process of sintered Ag paste, pores also simultaneously grow along with the migration of Ag particles, resulting in pores coarsening. To quantitatively evaluate microstructural variations, the pore sizes were measured by all the pore areas divided by the number of pores. The result of changing pore sizes during high temperature in air and in vacuum are shown in Fig. 3. After aging at 250 °C in air atmosphere, the average size of sintered Ag particles also became broader, extending from 0.96 μm to 2.55 μm as shown in Fig. 3(a). The average size of sintered Ag particles increased with thermal aging time up to 1000 h, while the particles growth indicated an exponential increase in air, and its trend was similar to that of general fine-grained materials. Fig. 3(b) quantitatively shows the variations in the pore sizes of sintered Ag paste under thermal aging. The average area of pores was used to represent pore size. The pore

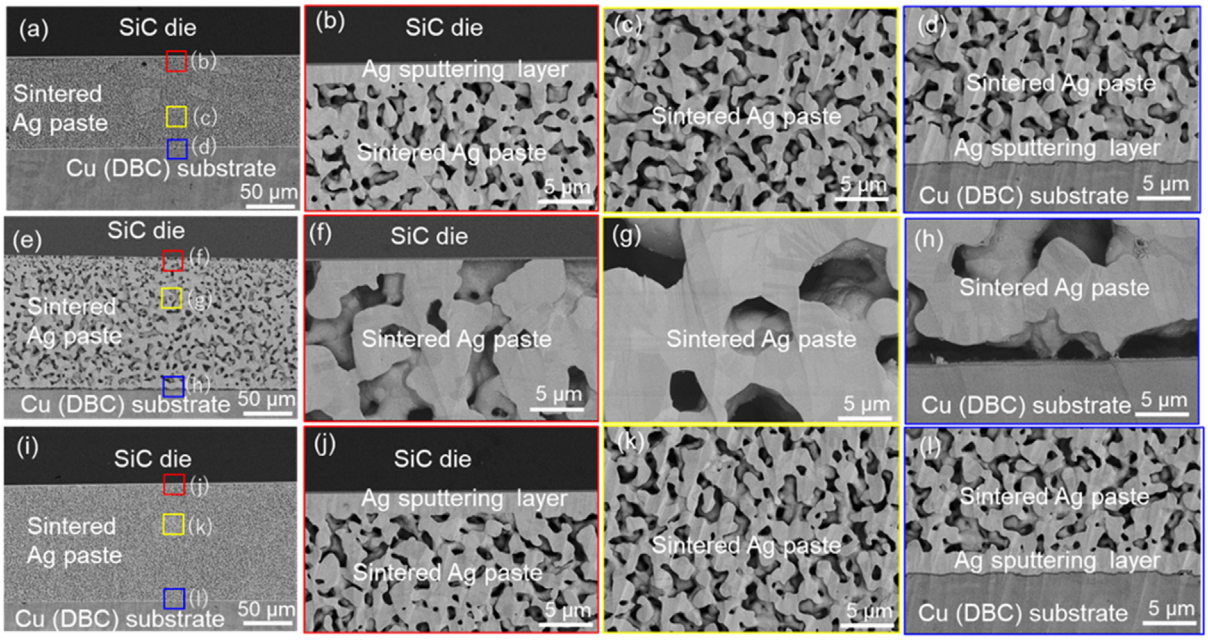

Fig. 2. (a) SEM images of the initial microstructure of the sintered Ag joint, the magnified views at (b) the interface of SiC and sintered Ag paste, (c) sintered porous Ag layer, and (d) the interface of sintered Ag paste and the DBC substrate, (e) The microstructure of the sintered Ag joint after aging at 250 °C for 500 h in air, and (f–h) are the magnified views at different locations, (i) the microstructure of the sintered Ag joint after aging at 250 °C for 500 h in vacuum, and (j–l) are the magnified views at different locations.

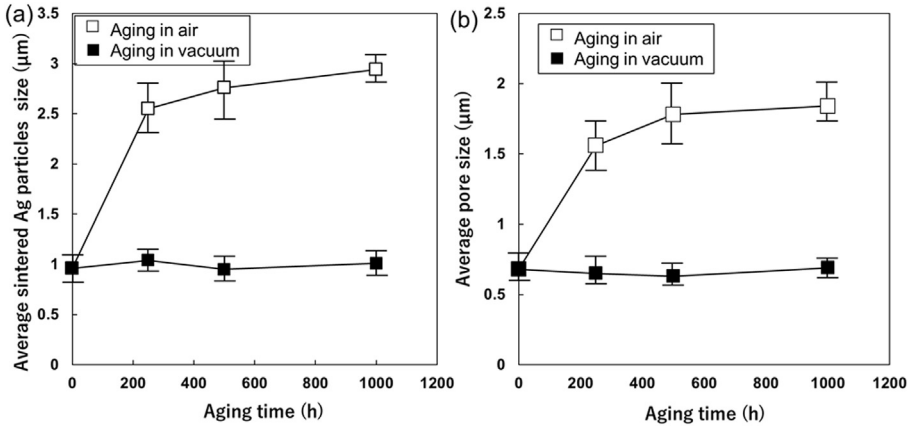

Fig. 3. (a) Sintered Ag particles size and (b) pore size of the microstructure of sintered Ag joint, before and after aging in air and vacuum atmospheres at 250 °C.

number at different thermal aging times was automatically counted by a software (Image- Pro Plus), and was expressed in percentiles based on the initial pore number. The pore size increased with increasing thermal exposure time, while the pore number decreased, and the most pore coarsening proceeded before 250 h.

However, in the vacuum aging, the microstructure remained almost unchanged as shown in Fig. 2(i), and the particles size had a mean value of approximately 1.04 μm after 1000 h. No clear coarsening behaviors occurred at the interface between the SiC chip and sintered Ag paste, the sintered Ag paste layer, and the interface of the sintered Ag paste and the Cu substrate, as shown in Fig. 2(j–l). Additionally, the Ag metallization did not diffuse into the sintered Ag paste as it did in air aging. Owing to the aging temperature and time were same as in air atmosphere, the key factor of the metallization layer diffusion and Ag particle coarsening phenomena were considered to be related with oxygen.

Theoretically, the particle growth induced by Ag self-diffusion can be estimated by the following equation [50,51]:

$$X_t - X_o = \sqrt{Dt} \quad (1)$$

where, D is the diffusion coefficient (m^2/s), X_t and X_o are particle sizes before and after aging (m), respectively, and t is the time under high-temperature aging treatment (s). The diffusion coefficient D was highly dependent on the aging temperature [52–54]. According to the equation, the self-diffusion coefficient of Ag was less than 3×10^{-22} m^2/s at approximately 250 °C. After calculation, the sintered Ag particles size was estimated to increase by approximately 45 nm after aging at 250 °C for 1000 h, and this did not agree with the changed state of Ag particles in air aged at 250 °C after 1000 h, as shown in Fig. 3. The reason can be contributed to the micron-porous structure of the sintered Ag joint. While particle growth depends on solid-solid contacts, the existence of pores decreased the contact area between adjacent particles, retarding necking interface migration. Although surface diffusion and particle boundary diffusion of Ag atoms did not consider in the equation

(1), the effect of vacuum on the coarsening behaviors of sintered Ag paste inhibitors was confirmed. The results indicated the self-diffusion kinetics of Ag may not be the main factor for the particle growth, and another mechanism is responsible for this rapid coarsening behavior of sintered Ag paste in air.

3.1.2. Particle coarsening mechanism

Further study was conducted through TEM (JEM-ARM200F, JEOL) to investigate the microstructure of the sinter Ag joint layer. Fig. 4 shows TEM images of sintered Ag paste before aging and after aging for 500 h in air and vacuum atmospheres. For the initial sinter Ag, the Ag particles were contacted together with necking growth as seen in Fig. 4(a) and its magnified view (Fig. 4(b)). The microstructure observed by TEM shows that the sintered Ag paste did not considerably change in the vacuum atmosphere as shown in Fig. 4(c) and (d). However, the case was completely different in the air atmosphere after aging. A large quantity of nanoparticles formed on the surfaces of Ag particles after aging in air for 500 h, and these nanoparticles formed a nanostructure among these Ag particles (Fig. 4(e)). In addition, nanoparticles also can be found at the particles interface necking and filled with some pore locations (see supporting information F. S2). Simultaneously, a liquid-like material with an amorphous structure was observed surrounding the nanoparticles and subsequently filled the pore of the sintered Ag paste. The high-resolution TEM image (Fig. 4(f)) showed that the average size of the nanoparticles was less than 10 nm. According to the EDS mapping analysis, the nanoparticles were composited by Ag and a litter of oxygen as seen in Fig. 4(g) and (h), respectively. The results indicated that the formation of Ag nanoparticles was closely related to the air atmosphere. Therefore, it was considered that these nanoparticles played a crucial role in the coarsening behaviors of the sintered Ag paste. In addition, because there are not any organic solvents residual on the Ag particles surface after sintering as shown in Fig. 4(a) and (b), the organic influence on the coarsening behaviors can be ignored.

The formation of Ag nanoparticles was previously reported in sintered Ag micron-sized flake particles [27,34], which was influenced by the grain boundary and dislocation density of the initial Ag particles, and recently, it was confirmed that oxygen plays a very important role in the formation of Ag nanoparticles [55]. As the sintered Ag joint was a porous structure, the oxygen can easily enter into the Ag joint during aging. Normally, oxygen atoms were preferentially absorbed or precipitated along Ag surfaces or grain boundaries [56,57], which would form an oxygen-rich region and increase the local oxygen partial pressures. In such oxygen-rich systems, previous research has confirmed that Ag would easily react with oxygen to form Ag_2O, and then, the partial pressure of oxygen decreased subsequently. Ag nanoparticles might be produced from an Ag-O reaction at 250 °C for a long time. However, according to the Ellingham diagrams and kinetics mechanism, the Ag_2O product was unstable at 250 °C and then decomposed to Ag and oxygen [58]. Thus, the formation of Ag nanoparticles, herein, was supposed to be caused by the thermal decomposition of the Ag_2O from the reaction between Ag and oxygen at 250 °C.

Based on the SEM and TEM observations, a possible mechanism of coarsening behaviors of sintered Ag paste aging in air was proposed in this study. First, the sintered Ag paste was a porous structure which was formed by Ag particles diffusion with necking growth during sintering as shown in Fig. 5(a). New Ag particle necking interfaces (Ag grain boundaries) are formed by Ag particles connection and local particles growth or shrinkage, where, in addition to a large Ag particle interfaces density, oxygen can enter into the porous Ag structure via the Ag particle interfaces during aging. The microscopic schematic of sintered Ag paste without pore can be considered and seen in Fig. 5(b). Second, from the reaction between Ag and oxygen at 250 °C, Ag_2O was formed at the Ag particle necking interfaces as shown in Fig. 5(c). Eventually, Ag nanoparticles were generated from the Ag particle necking interfaces, induced by the thermal decomposition of the Ag_2O. When the Ag nanoparticles were in-situ formed in air during aging at 250 °C, they were accompanied with large Ag particles to become a "bimodal Ag particles system" as shown in Fig. 5(d). The system stayed in a thermodynamically unstable state because the nanoparticles possessed a very high surface energy and lower melting point because of their higher molar surface area compared with large Ag particles. Finally, to reach an equilibrium state, the

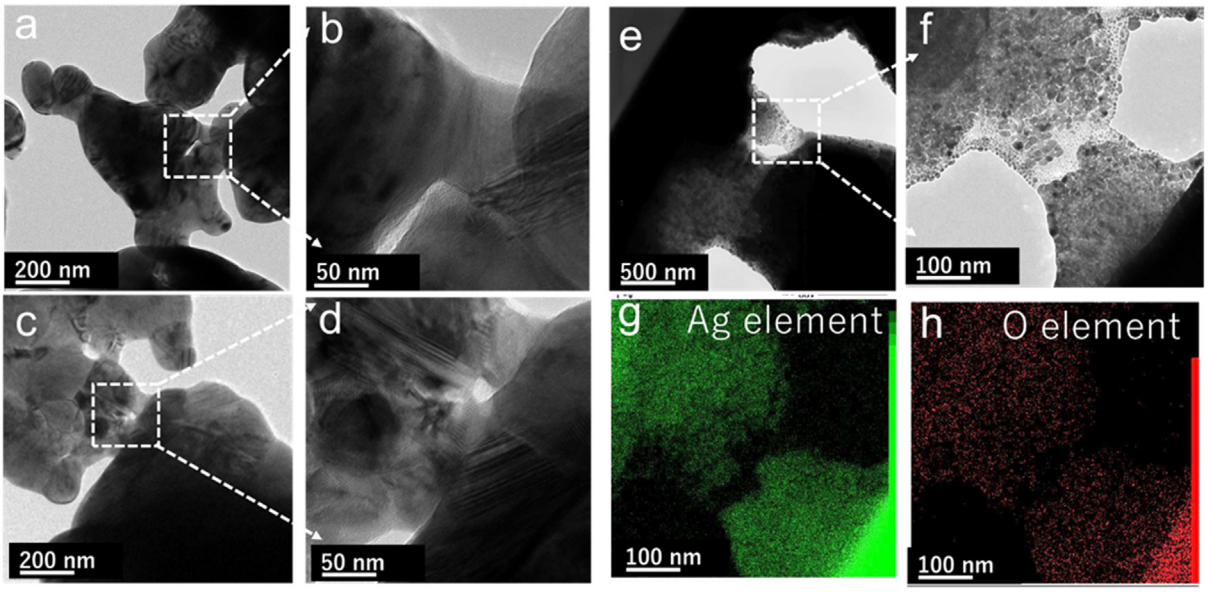

Fig. 4. (a) TEM image of the microstructure of the initial sintered Ag particle, (b) local magnified image, (c) after aging in vacuum at 250 °C for 500 h, (d) the local magnified image, (e) microstructure of the sintered Ag particles after aging in air at 250 °C for 500 h, and (f) Ag nanoparticles formed around sintered Ag particles, (g) the EDX element mapping of Ag atoms, (h) the EDX element mapping of O atoms.

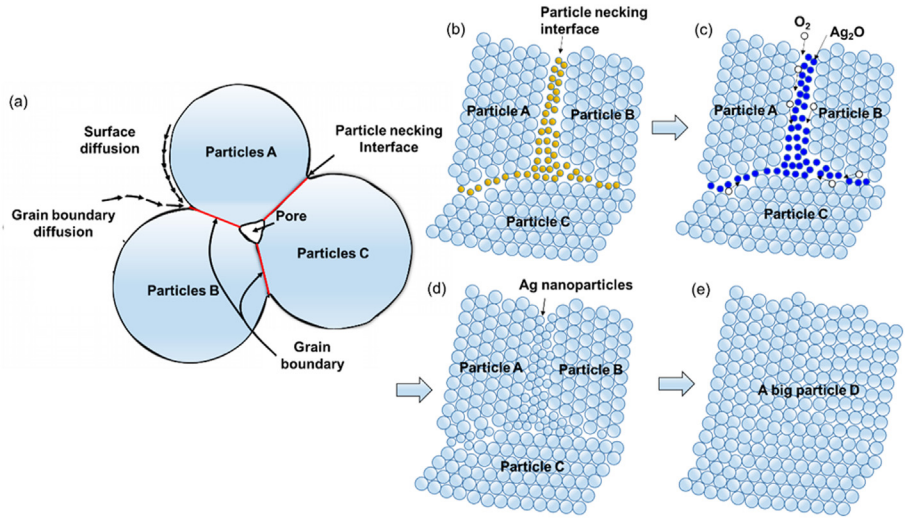

Fig. 5. A possible mechanism of coarsening behavior: (a) sintered Ag paste structure by several Ag particles with necking growth, (b) microscopic schematic of sintered Ag paste without pore, (c) Ag_2O was formed at the Ag particle necking interfaces, (d) Ag nanoparticles generated from the Ag particle necking interfaces by the thermal decomposition of the Ag_2O, (e) Ag particles changed to one big Ag particles caused by minimizing the surface energy of the Ag nanoparticles.

nanoparticles will coalesce into large Ag particles through minimizing the surface energy and finally change the Ag particles and necking growth to a bigger size as shown in Fig. 5(e). These Ag nanoparticles served as a nano-bridge among these large particles to improve grain boundary diffusion behaviors [59]. However, in vacuum, the Ag particles were almost constant with the initial sizes due to the slow thermal self-diffusion of Ag. Thus, the coarsening behaviors of sintered Ag paste may be mainly controlled by in situ nanoparticles information rather than thermal Ag self-diffusion at 250 °C aging.

3.2. Fracture behaviors of sinter Ag joint

3.2.1. Die shear strength

Fig. 6 shows the die shear strength of the sintered Ag joint after different aging times in air and vacuum atmospheres. The initial shear strength was 17.9 MPa and it did not change significantly in both air (17.6 MPa) and vacuum (18.1 MPa) atmospheres after aging for 1000 h. The die shear strength is increased to a different point after aging 250 h in air but only slightly decreases in vacuum. The increase in air aging may be attributed to the re-sintering process [60]. Due to interface connection ratio did not so much change during the aging process in air for the case of sputtered Ag metallization [47, the shear strength did not change much after aging for 500 h, and even 1000 h. Additionally, because the microstructure and the Ag metallization layer almost remained constant during aging in the vacuum atmosphere, the shear strength maintained its initial value and was not influenced by the high-temperature environment. As the actual power modules were packaged by a resin, which was isolated from the oxygen, the power module by the sintered Ag joint provides an excellent thermally stable reliability.

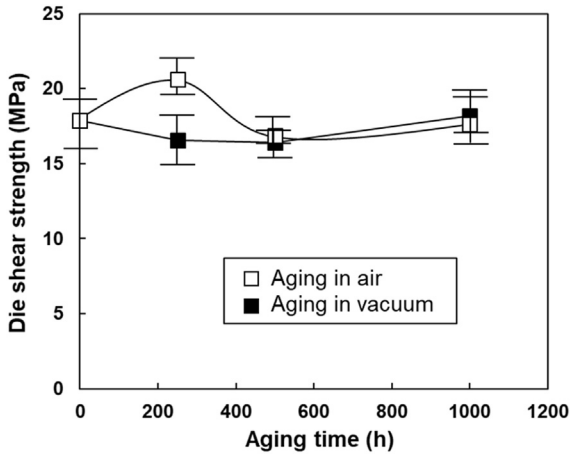

Fig. 6. The die shear strength of the sintered Ag joint structure after aging in air and vacuum.

3.2.2. Fracture behaviors

Fig. 7 shows the SEM image of the fracture surface of the initial sintered Ag joint structure and aging at 250 °C for 500 h in air and in vacuum. The white arrow represents the direction of the shear load. The initial sintered Ag joint was fractured at the inner part of the sintered Ag layer as shown in Fig. 7(a). A large deformation appeared at Ag particle necking as shown in the magnified view of Fig. 7(b) and (c). Fig. 7(d) shows the fracture surface of sintered Ag joint after aging at 250 °C for 500 h in air. Fig. 7(e) was the local magnify view. It was found that the fracture mode changed to the bonded-line interface between the chip and sintered Ag to the interface between sintered Ag and substrate after aging in air. Particle coarsening could be found from the fracture surface, where the size of Ag particle necking (see Fig. 7(f)) was larger than that initial sintered Ag joint.

Fig. 7(g) shows the fracture surface of the sintered Ag joint after aging at 250 °C for 500 h in vacuum. Fig. 7(h) was the local magnify view. The fracture was the same as the initial sintered Ag joint from the inner part of the sintered Ag layer with a large deformation at the Ag particle necking. In addition, no clearly growth occurred at the Ag particle necking in vacuum (see Fig. 7(i)). The schematic diagram of fracture mode of the initial sintered Ag joint before and after aging at 500 h in air were shown in Fig. 7(j) and (k), respectively. The Ag metallization diffused into the sintered porous Ag during the aging as shown in Fig. 2(f) and (h), leading to the sintered porous Ag was directly bonded with the Ti metallization layer, which may cause the change in the fracture mode. Fig. 7(l) shows the fracture mode after aging for 500 h in vacuum where the Ag metallization layer did not diffuse into the sintered porous Ag.

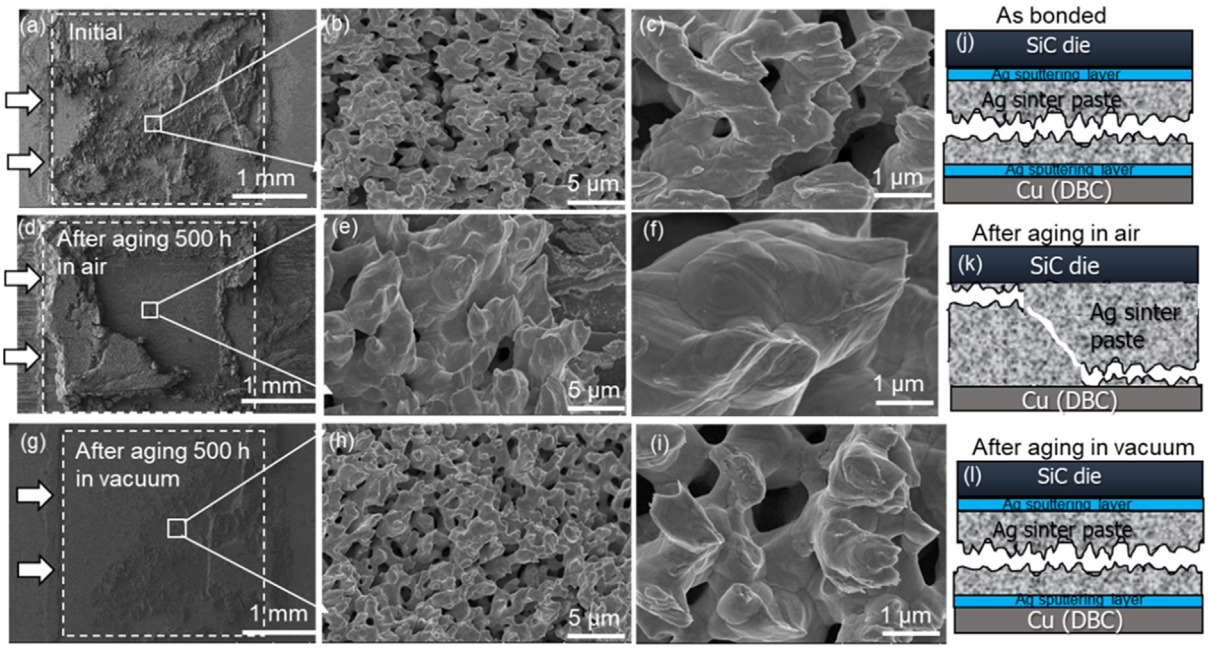

Fig. 7. SEM image of fracture surface of the initial sinter Ag joint structure (a–c) before and (d–f) after aging at 250 °C for 500 h in air, (g–i) after aging 500 h in vacuum, the schematic diagram of the fracture mode of the initial sinter Ag joint (j) and (k) after aging for 500 h in air and (l) in vacuum.

3.3. Micromechanical properties

3.3.1. Nanoindentation response

Fig. 8 shows the load-displacement curve of the sintered porous Ag aging for different times. All the load-displacement curves firstly show a continuous increment in displacement, corresponding to the applied load increments. This result indicates that the indentation depth increases until plastic deformation of the sintered porous Ag is achieved. The curve shows a decrease of the indentation depth that is attributable to the elastic recovery, when the load is gradually removed. It can be seen that the displacement increased after aging for 250 h in air, and then decreased even less than the initial sintered porous Ag after aging for 1000 h as seen in Fig. 8(a). The micromechanical properties of the sintered porous Ag depend on the load-displacement curve, which is influenced by the aging process in air. On the other hand, the displacement did not considerably change, and the disorder with the aging time during the vacuum aging is depicted in Fig. 8(b).

Fig. 9(a) shows the SEM image of top view of indentation on the surface of sintered Ag paste aged for 500 h in air. The image was obtained at a tilted angle of 40°. In order to gain a further understanding of the deformation behaviors during the indentation test, the cross-section of the microstructural after the indentation was fabricated using FIB milling process as shown in Fig. 9(b). In previous study, the deformed area underneath the indentation of a porous ceramic films was divided into four rectangular shapes with identical height and width, which was equivalent to the diameter of the projected circular area of the indent [61]. The plastic zone was a crushed region having higher density. Based on this theory, the plastic zone in this study was the area enclosed by red dotted line as seen in Fig. 9(b). The magnified view of microstructure under the indentation was shown in Fig. 9(c), where sintered Ag paste become dense due to the large compressive deformation during the test. Fig. 9(d) and (e) show top view of indentation of sintered Ag paste aged for 500 h in vacuum and its cross-section image, respectively. A dense area also appeared after the indentation test as shown in Fig. 9(f). The plastic zone size corresponds to the load-displacement curve response and influence the micromechanical properties.

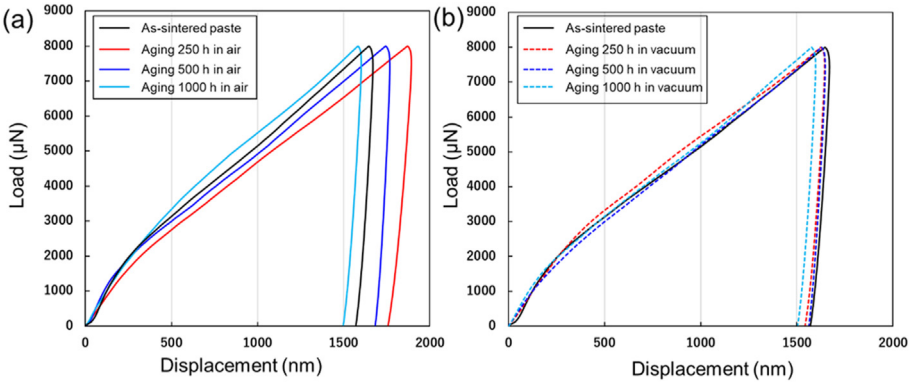

Fig. 8. Load-displacement curve of sintered porous Ag aging (a) in air and (b) in vacuum for different times.

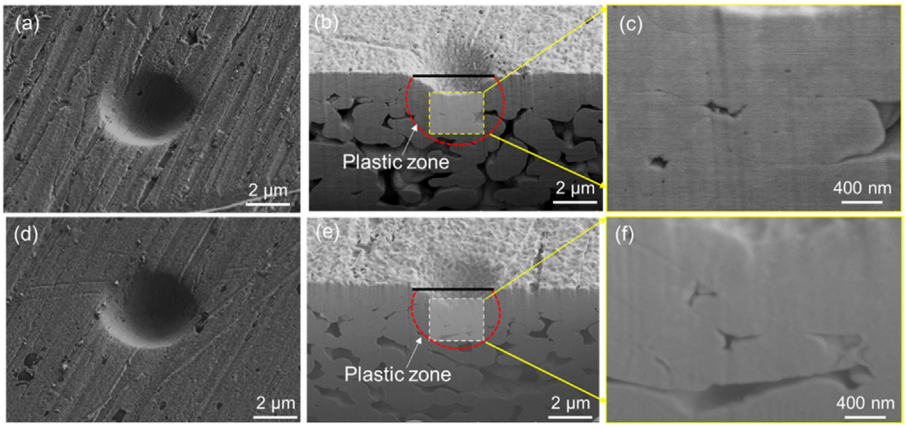

Fig. 9. (a) The top view of indentation on the surface of sintered Ag aged for 500 h in air and (d) in vacuum, (b) (e) FIB milled cross-sections and (c) (f) dense Ag microstructure under the indentation.

3.3.2. Micromechanical characterization

The loading stage represents the material hardness, which is defined by the ratio between the indentation load P and the contact area A. According to the Oliver-Pharr method [62], the applied load P on the indenter during the loading stage is directly associated with the material hardness H by the following equation:

$$H = \frac{P_{max}}{A} \tag{2}$$

The elastic modulus, E, of the materials is related to the materials' reduced modulus, E_r. Both moduli can be calculated by the following equations:

$$\mathrm{E} = \frac{1-\nu^2}{\frac{1}{E_r} - \frac{1-\nu_i^2}{E_i}} \tag{3}$$

$$E_r = \frac{S}{2a_n} \tag{4}$$

where, ν is the Poisson's ratio of the specimen. E_i and V_i are the elastic modulus and Poisson's ratio of the indenter, respectively. Herein, the Poisson's ratio of the sintered Ag paste was adopted from our previous study, where the Poisson's ratio was calculated as 0.31 at room temperature of 25 °C [63]. Fig. 10(a) shows the elastic modulus of the sintered porous Ag before and after aging for 250 h, 500 h, and 1000 h in air, which were calculated as 23.6 GPa, 19.9 GPa, 24.2 GPa, and 22.5 GPa, respectively. The elastic modulus largely decreased from the initial to 250 h, and recovery after aging for 500 h. On the other hand, the elastic modulus of the sintered porous Ag after aging for 250 h, 500 h, and 1000 h in vacuum were calculated as 22.6 GPa, 21.7 GPa, and 22.1 GPa, respectively. There was almost no change during the aging process. Additionally, the hardness of the sintered porous Ag also appeared with the same tendency as the elastic modulus during the aging process in air and in vacuum as seen in Fig. 10(b). Thus, the micromechanical properties of the sintered porous Ag, including the elastic modulus and hardness depend on its microstructure. However, as shown in Fig. 3, because both the sintered Ag particle size and pore size were gradually increased from the initial to 1000 h, there was no clear correlation between the sintered Ag particle size or pore size with the micromechanical properties of the sintered porous Ag.

Fig. 11(a) shows the variation in the porosities of the sintered Ag paste during thermal aging times in air and in vacuum. Porosity was measured by calculating the ratio of the pore area to the observed area based on the SEM image with different aging time (see supporting information F. S3). The monochrome image of the microstructure of the sintered porous Ag for 0, 250, 500, and 1000 h in air are shown in Fig. 11(b), (c), (d), and (e), respectively. The porosities of the sintered Ag that was exposed for 0, 250, 500, and 1000 h were 39%, 30%, 33%, and 34%, respectively. The porosity of the sintered Ag firstly decreased from the initial to 250 h, and then slightly increased. Previous studies have reported that when the sintered porous Ag is exposed to high temperatures at the initial stage, its porosity reduction is generated by a driving force to reduce surface energy [64,65]. On the other hand, it was found that the tendency of porosity change was similar to that of the micromechanical properties of the sintered porous Ag aging in air.

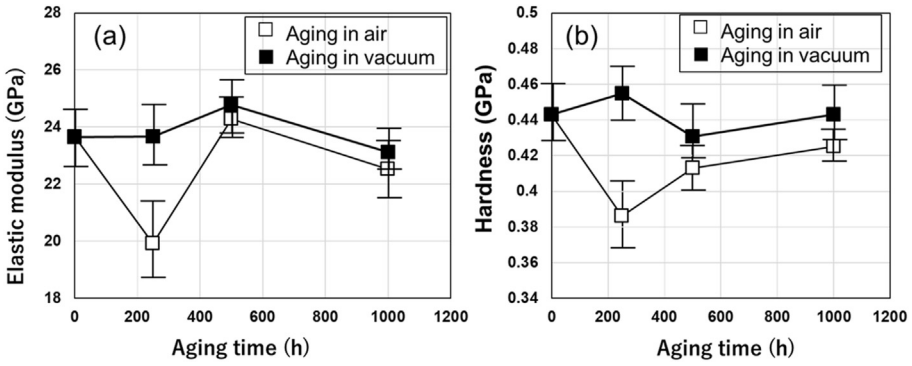

Fig. 10. (a) Elastic modulus and (b) the hardness of the sintered porous Ag aging in air and vacuum for different times.

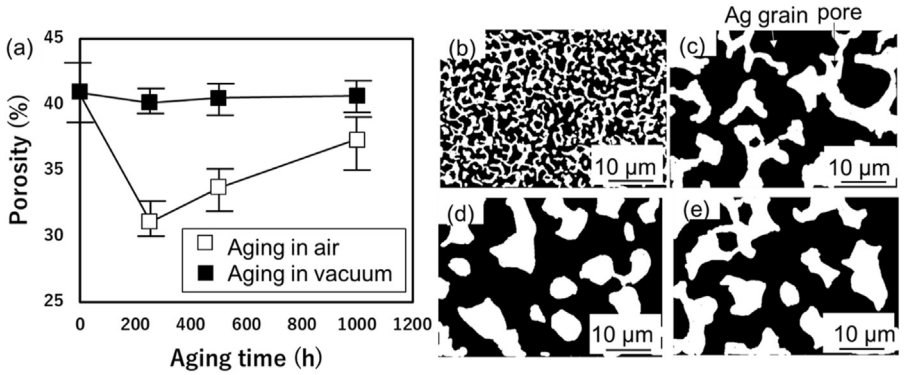

Fig. 11. (a) Porosity change of the sintered porous Ag during aging in air and vacuum, (b), (c), (d), and (e) are the monochrome images of the microstructure of the sintered porous Ag for 0, 250, 500, and 1000 h in air, respectively.

Therefore, the micromechanical properties of the sintered porous Ag should be largely influenced by its porosity as reported in previous studies [66–68].

4. Conclusions

This study systematically investigated the effect of oxygen on structural characterizations and mechanical properties of sintered Ag paste during high-temperature storage from macro to micro. Sintered Ag paste become coarsened after aging at 250 °C in air, but remain unchanged in a vacuum atmosphere at the same temperature. The mechanism of coarsening behaviors was revealed wherein oxygen plays an important role rather than the traditional Ag thermal self-diffusion. The Ag nanoparticles formed around the Ag particles are responsible for the difference, which was related to complex Ag-O reactions at the Ag particle necking interfaces. These Ag nanoparticles may serve as a nano-bridge among these large particles to improve particle boundary diffusion behaviors. Additionally, the micromechanical properties of the sintered Ag paste, including the elastic modulus and hardness, depend on its microstructure and are largely influenced by its porosity, which decreased remarkably from the initial to 250 h, and recovers after aging for 500 h in air but was almost unaltered during the aging process in vacuum. These results indicated that sintered Ag paste can be used as a reliable die attach material in high-temperature applications for WBG power modules, especially those packaged by a resin.

Author contributions

C. C, Z.Z completed the sinter Ag joining, high temperature aging and nanoindentation experiments, and studies reported in this work with technical guidance from F. W, N.S and K.S. X.L provided the design of nanoindentation experiments. Some SEM observation experiments were performed by C. C, D.K and Z.Z. The manuscript was written by C. C. with contributions from all other authors.

Declaration of competing interest

The authors declare that they have no known competing financial interests or personal relationships that could have appeared to influence the work reported in this paper.

We confirm that this manuscript has not been published elsewhere and is not under consideration inwhole or in part by another journal. All authors have approved the manuscript and agree with submission to Journal of alloy and compounds. All data is true and reliable. The authors have no conflicts of interest to declare.

CRediT authorship contribution statement

Chuantong Chen: Data curation, Writing - review & editing, Conceptualization, Methodology, Investigation, Writing - original draft. **Chanyang Choe:** Data curation, Writing - review & editing. **Dongjin Kim:** Data curation, Writing - review & editing. **Zheng Zhang:** Data curation, Writing - review & editing, Validation, Formal analysis. **Xu Long:** Data curation, Writing - review & editing, Formal analysis. **Zheng Zhou:** Data curation, Writing - review & editing, Validation, Formal analysis. **Fengshun Wu:** Resources, Data curation, Writing - review & editing, Supervision. **Katsuaki Suganuma:** Resources, Writing - review & editing, Supervision, Data curation.

Acknowledgements

This work was supported by the JST Advanced Low Carbon Technology Research and Development Program (ALCA) project “Development of a high frequency GaN power module package technology”, (Grant No. JPMJAL1610). This work was also partly supported by the Japan Society for the Promotion of Science (JSPS) Grant-in-Aid for Scientific Research (Grant No. 19121587).

Appendix A. Supplementary data

Supplementary data to this article can be found online at https://doi.org/10.1016/j.jallcom.2020.155173.

References

[1] P.G. Neudeck, R.S. Okojie, L.-Y. Chen, High-temperature electronics a role for wide bandgap semiconductors, Proc. IEEE 90 (2002) 1065–1076.
[2] H.S. Chin, K.Y. Cheong, A.B. Ismail, A review on die attach materials for SiC-based high-. temperature power devices, Met. Mat. Trans., B. 41 (2010) 824–832.
[3] S.H. Ryu, B.A. Hull, S. Dhar, L. Cheng, Q.C.J. Zhang, J. Richmond, M.K. Das, A.K. Agarwal, J.W. Palmour, A.J. Lelis, B. Geil, C. Scozzie, Performance, Reliability, and robustness of 4H-SiC power DMOSFETs, Mater. Sci. Forum 645–648 (2010) 969–974.
[4] E. Ide, S. Angata, A. Hirose, K.F. Kobayashi, Metal-metal bonding process using Ag metallo-organic nanoparticles, Acta Mater. 53 (2005) 2385–2393.
[5] C. Chen, S. Noh, H. Zhang, C. Choe, J. Jiu, S. Nagao, K. Suganuma, Bonding technology based on solid porous Ag for large area chip, Scripta Mater. 146 (2018) 123–127.
[6] K.S. Siow, Mechanical properties of nano-silver joints as die attach materials, J. Alloys Compd. 514 (2012) 6–19.
[7] K. Suganuma, S. Sakamoto, N. Kagami, D. Wakuda, K.S. Kim, M. Nogi, Low-temperature low-pressure die attach with hybrid silver particle paste, Microelectron. Reliab. 52 (2012) 375–380.
[8] K.S. Siow, Y.T. Lin, Identifying the development state of sintered silver (Ag) as a bonding material in the microelectronic packaging via a patent landscape study, J. Electron. Packag. 138 (2016), 020804.
[9] J. Yan, G. Zou, A.-P. Wu, J. Ren, J. Yan, A. Hu, Y. Zhou, Pressureless bonding process using Ag nanoparticle paste for flexible electronics packaging, Scripta

Mater. 66 (2012) 582–585.
[10] C. Chen, S. Nagao, K. Suganuma, J. Jiu, H. Zhang, T. Sugahara, T. Iwashige, K. Sugiura, K. Tsuruta, Self-healing of cracks in Ag joining layer for die-attachment in power devices, Appl. Phys. Lett. 109 (2016), 093503.
[11] C. Chen, C. Choe, Z. Zhang, D. Kim, K. Suganuma, Low-stress design of bonding structure and its thermal shock performance (-50 to 250 °C) in SiC/DBC power die-attached modules, J. Mater. Sci. Mater. Electron. 29 (2018) 14335–14346.
[12] D. Kim, C. Chen, S. Noh, S.-J. Lee, Z. Zhang, Y. Kimoto, T. Sugahara, K. Suganuma, Development of high-strength and superior thermal shock-resistant GaN/DBA die attach structure with Ag sinter joining by thick Ni metallization, Microelectron. Reliab. 100–101 (2019), 113380.
[13] Z. Zhang, C. Chen, Y. Yang, H. Zhang, D. Kim, T. Sugahara, S. Nagao, K. Suganuma, Low-temperature and pressureless sinter joining of Cu with micron/submicron Ag particle paste in air, J. Alloys Compd. 780 (2019) 435–442.
[14] S. Zabihzadeh, S. Van Petegem, L.I. Duarte, R. Mokso, A. Cervellino, H. Van Swygenhoven, Deformation behavior of sintered nanocrystalline silver layers, Acta Mater. 97 (2015) 116–123.
[15] S.T. Chua, K.S. Siow, Microstructural studies and bonding strength of pressureless sintered nano-silver joints on silver, direct bond copper (DBC) and copper substrates aged at 300°C, J. Alloys Compd. 687 (2016) 486–498.
[16] P. Gadaud, V. Caccuri, D. Bertheau, J. Carr, X. Milhet, Ageing sintered silver: relationship between tensile behavior, mechanical properties and the nano-porous structure evolution, Mater. Sci. Eng. 669 (2016) 379–386.
[17] S.A. Paknejad, G. Dumas, G. West, G. Lewis, S.H. Mannan, Microstructure evolution during 300 °C storage of sintered Ag nanoparticles on Ag and Au substrates, J. Alloys Compd. 617 (2014) 994–1001.
[18] R. Khazaka, L. Mendizabal, D. Henry, Review on joint shear strength of nano-silver paste and its long-term high temperature reliability, J. Electron. Mater. 43 (2014) 2459–2466.
[19] J.G. Bai, G.Q. Lu, Thermomechanical reliability of low-temperature sintered silver die attached SiC power device assembly, IEEE Trans. Device Mater. Reliab. 6 (2006) 436–441.
[20] H. Zhang, C. Chen, S. Nagao, K. Suganuma, Thermal fatigue behavior of silicon-carbide-doped silver microflake sinter joints for die attachment in silicon/silicon carbide power devices, J. Electron. Mater. 46 (2017) 1055–1060.
[21] C. Choe, S. Noh, C. Chen, D. Kim, K. Suganuma, Influence of thermal exposure upon mechanical/electrical properties and microstructure of sintered micro-porous silver, Microelectron. Reliab. 88–90 (2018) 695–700.
[22] X. Milhet, P. Gadaud, V. Caccuri, D. Bertheau, D. Mellier, M. Gerland, Influence of the porous microstructure on the elastic properties of sintered Ag paste as replacement material for die attachment, J. Electron. Mater. 44 (2015) 3948–3956.
[23] S. Sakamoto, T. Sugahara, K. Suganuma, Microstructural stability of Ag sinter joining in thermal cycling, J. Mater. Sci. Mater. Electron. 24 (2013) 1332–1340.
[24] E.H. Baker, J.K. Johnstone, Effect of oxygen pressure on the melting of silver, Nature 205 (1965) 65–66.
[25] S.K. Lin, S. Nagao, E. Yokoi, C. Oh, H. Zhang, Y.C. Liu, S.G. Lin, K. Suganuma, Nano-volcanic eruption of silver, Sci. Rep-UK. 6 (2016), 34769.
[26] P. Christopher, H. Xin, S. Linic, Visible-light-enhanced catalytic oxidation reactions on plasmonic silver nanostructures, Nat. Chem. 3 (2011) 467–472.
[27] N. Matsuhisa, D. Inoue, P. Zalar, H. Jin, Y. Matsuba, A. Itoh, T. Yokota, D. Hashizume, T. Someya, Printable elastic conductors by in situ formation of silver nanoparticles from silver flakes, Nat. Mater. 16 (2017) 834–840.
[28] C. Oh, S. Nagao, K. Suganuma, Silver stress migration bonding driven by thermomechanical stress with various substrates, J. Mater. Sci. Mater. Electron. 26 (2015) 2525–2530.
[29] S.J. Noh, C. Choe, C. Chen, K. Suganuma, Heat-resistant die-attach with cold-rolled Ag sheet, Appl. Phys. Express. 11 (2018), 016501.
[30] C. Oh, S. Nagao, T. Sugahara, K. Suganuma, Hillock growth dynamics for Ag stress migration bonding, Mater. Lett. 137 (2014) 170–173.
[31] C. Oh, S. Nagao, T. Kunimune, K. Suganuma, Pressureless wafer bonding by turning hillocks into abnormal particle growths in Ag films, Appl. Phys. Lett. 104 (2014), 161603.
[32] C. Chen, S. Nagao, K. Suganuma, J. Jiu, T. Sugahara, H. Zhang, T. Iwashige, K. Sugiura, K. Tsuruta, Macroscale and microscale fracture toughness of microporous sintered Ag for applications in power electronic devices, Acta Mater. 129 (2017) 41–51.
[33] A.H. Almasri, G.Z. Voyiadjis, Nano-indentation in FCC metals: experimental study, Acta Mater. 209 (2010) 1–9.
[34] C. Chen, K. Suganuma, Microstructure and mechanical properties of sintered Ag particles with flake and spherical shape from nano to micro size, Mater. Des. 162 (2019) 311–321.
[35] J.R. Greer, Warren C. Oliver, William D. Nix, Size dependence in mechanical properties of gold at the micron scale in the absence of strain gradients, Acta Mater. 53 (2005) 1821–1830.
[36] K.J. Hemker, W.N. Sharpe Jr., Microscale characterization of mechanical properties, Annu. Rev. Mater. Res. 37 (2007) 93–126.
[37] B. Poon, D. Rittel, G. Ravichandran, An analysis of nanoindentation in linearly elastic solids, Int. J. Solid Struct. 45 (2008) 6018–6033.
[38] W.C. Oliver, G.M. Pharr, Measurement of hardness and elastic modulus by instrumented indentation: advances in understanding and refinements to methodology, J. Mater. Res. 19 (2004) 3–20.
[39] X. Long, B. Hu, Y. Feng, C. Chang, M. Li, Correlation of microstructure and constitutive behaviour of sintered silver particles via nanoindentation, Int. J. Mech. Sci. 161–162 (2019), 105020.
[40] X. Long, Z. Li, X. Lu, H. Guo, C. Chang, Q. Zhang, A. Zehri, W. Ke, Y. Yao, L. Ye, J. Liu, Mechanical behaviour of sintered silver nanoparticles reinforced by SiC microparticles, Mater. Sci. Eng. 744 (2019) 406–414.
[41] K.-S. Moon, H. Dong, R. Maric, S. Pothukuchi, A. Hunt, Y. Li, C.P. Wong, Thermal behavior of silver nanoparticles for low temperature interconnect applications, J. Electron. Mater. 34 (2005) 168–175.
[42] J. Jiu, H. Zhang, S. Koga, S. Nagao, Y. Izumi, K. Suganuma, Simultaneous synthesis of nano and micro-Ag particles and their application as a die-attachment material, J. Mater. Sci. Mater. Electron. 26 (2015) 7183–7191.
[43] J. Jiu, H. Zhang, S. Nagao, T. Sugahara, N. Kagami, Y. Suzuki, Y. Akai, K. Suganuma, Die-attaching silver paste based on a novel solvent for high-power semiconductor devices, J. Mater. Sci. 51 (2016) 3422–3430.
[44] A. Leitner, V. M-Kiener, D. Kiener, Essential refinements of spherical nano-indentation protocols for the reliable determination of mechanical flow curves, Mater. Des. 146 (2018) 69–80.
[45] Z. Chen, X. Wang, A. Atkinson, N. Brandon, Spherical indentation of porous ceramics: elasticity and hardness, J. Eur. Ceram. Soc. 36 (2016) 1435–1445.
[46] H. Zhang, S. Nagao, K. Suganuma, H.J. Albrecht, K. Wilke, Thermostable Ag die-attach structure for high-temperature power devices, J. Mater. Sci. 27 (2016) 1337–1344.
[47] C. Chen, K. Suganuma, T. Iwashige, K. Sugiura, K. Tsuruta, High-temperature reliability of sintered microporous Ag on electroplated Ag, Au, and sputtered Ag metallization substrates, J. Mater. Sci. Mater. Electron. 29 (2018) 1785–1797.
[48] S.R. Challa, A.T. Delariva, T.W. Hansen, S. Helveg, J. Sehested, P.L. Hansen, F. Garzon, A.K. Datye, Relating rates of catalyst sintering to the disappearance of individual nanoparticles during Ostwald ripening, J. Am. Chem. Soc. 133 (2011) 20672–20675.
[49] W.D. Kingery, B. Francois, Particle growth in porous compacts, J. Am. Ceram. Soc. 48 (1965) 546–547.
[50] J.C. Fisher, Calculation of diffusion penetration curves for surface and particle boundary diffusion, J. Appl. Phys. 22 (1951) 74–77.
[51] P.M. Agrawal, B.M. Rice, D.L. Thompson, Predicting trends in rate parameters for self-diffusion on FCC metal surfaces, Surf. Sci. 515 (2002) 21–35.
[52] N.H. Nachtrieb, Structure of liquid metals, Adv. Phys. 16 (1967) 309–323.
[53] R.E. Hoffman, D. Turnbull, Lattice and particle boundary self-diffusion in silver, J. Appl. Phys. 22 (1951) 634–639.
[54] W.C. Mallard, A.B. Gardner, R.F. Bass, L.M. Slifkin, Self-diffusion in silver-gold solid solutions, Phys. Rev. 129 (1963) 617–625.
[62] C. Chen, J. Yeom, C. Choe, G. Liu, Y. Gao, Z. Zhang, B. Zhang, D. Kim, K. Suganuma, Necking growth and mechanical properties of sintered Ag particles with different shapes under air and N_2 atmosphere, J. Mater. Sci. 54 (2019) 13344–13357.
[55] T. Schuh, H. Hahn, H. Gleiter, Particle boundary structure and boundary segregation in AgO alloys, Mater. Sci. Eng. 84 (1986) 191–193.
[56] J. Assal, B. Hallstedt, L.J. Gauckler, Thermodynamic assessment of the silver-oxygen system, J. Am. Ceram. Soc. 80 (1997) 3054–3060.
[57] H. Zhang, Y. Gao, J. Jiu, K. Suganuma, In situ bridging effect of Ag_2O on pressureless and low-temperature sintering of micron-scale silver paste, J. Alloys Compd. 696 (2017) 123–129.
[58] J. Yeom, S. Nagao, C. Chen, T. Sugahara, H. Zhang, C. Choe, C.-F. Li, K. Suganuma, Ag particles for sinter bonding: flakes or spheres? Appl. Phys. Lett. 114 (2019), 253103.
[59] H. Zhang, C. Chen, J. Jiu, S. Nagao, K. Suganuma, High-temperature reliability of low-temperature and pressureless micron Ag sintered joints for die attachment in high-power device, J. Mater. Sci. Mater. Electron. 29 (2018) 8854–8862.
[60] Z. Chen, X. Wang, V. Bhakhri, F. Giuliani, A. Atkinson, Nanoindentation of porous bulk and thin films of La0.6Sr0.4Co0.2Fe0.8O3−δ, Acta Mater. 61 (2013) 5720–5734.
[61] W.C. Oliver, G.M. Pharr, An improved technique for determining hardness and elastic modulus using load and displacement sensing indentation experiments, J. Mater. Res. 7 (1992) 1564–1583.
[63] C. Chen, S. Nagao, H. Zhang, J. Jiu, T. Sugahara, K. Suganuma, T. Iwashige, K. Sugiura, K. Tsuruta, Mechanical deformation of sintered porous Ag die attach at high temperature and its size effect for wide-bandgap power device design, J. Electron. Mater. 46 (2017) 1576–1586.
[64] J.D. Osorio, D. Maya, A.C. Barrios, A. Lopera, F. Jiménez, J.M. Meza, J.P. Hernández-Ortiz, A. Toro, Correlations between microstructure and mechanical properties of air plasma-sprayed thermal barrier coatings exposed to a high temperature, J. Am. Ceram. Soc. 96 (2013) 3901–3907.
[65] C. Choe, S. Noh, C. Chen, D. Kim, K. Suganuma, Influence of thermal exposure upon mechanical/electrical properties and microstructure of sintered micro-porous silver, Microelectron. Reliab. 88–90 (2018) 695–700.
[66] J. Carr, X. Milhet, P. Gadaud, S.A.E. Boyer, G.E. Thompson, P. Lee, Quantitative characterization of porosity and determination of elastic modulus for sintered micro-silver joints, J. Mater. Process. Technol. 225 (2015) 19–23.
[67] V. Caccuri, X. Milhet, P. Gadaud, D. Bertheau, M. Gerland, Mechanical properties of sintered ag as a new material for die bonding: influence of the density, J. Electron. Mater. 43 (2014) 4510–4514.
[68] P. Gadaud, V. Caccuri, D. Berthau, J. Carr, X. Milhet, Ageing sintered silver: relationship between tensile behavior, mechanical properties and the nano porous structure evolution, Mater. Sci. Eng. 669 (2016) 379–386.